*sustainability*

MDPI

*Article*

# Numerical Simulation of Thermal Storage Performance of Different Concrete Floors

**Yudi Wang and Guoqiang Xu ***

Green Building Autonomous Region Key Laboratory of Higher Education, School of Architecture, Inner Mongolia University of Technology, Hohhot 010051, China
* Correspondence: xgq5@imut.edu.cn; Tel.: +86-471-6576170

**Abstract:** To improve the utilization rate of energy, the consumption of fossil energy must be reduced. In this study, a low-temperature radiant floor made of concrete is taken as the research object, and a two-dimensional low-temperature hot water radiant heating system with different concrete filling layers is numerically simulated using a computational fluid dynamics (CFD) software and finite element method. In this numerical model, a concrete sensible heat storage (SHTES) is adopted, while various types of concrete materials have been used to preliminarily analyze the influence of different concrete types on floor heat storage. The simulation results were further analyzed to determine the total heat storage during the heating period and the total heat storage and heat storage rate during the stable operation stage. The results demonstrate that the thermal conductivity coefficient of concrete floors had the most significant influence on the heat storage effect, with slag concrete demonstrating the most prominent heat storage effect. The total heat storage capacity of slag concrete after 7 h was 848.512 J. Overall, this study proposes a method to enhance the heat storage capacity of low-temperature radiant floors, while providing a design method for future solar energy storages and floor heat storages.

**Keywords:** concrete; low temperature radiant floor; sensible heat storage; simulation; computational fluid dynamics



**Citation:** Wang, Y.; Xu, G. Numerical Simulation of Thermal Storage Performance of Different Concrete Floors. *Sustainability* **2022**, *14*, 12833. https://doi.org/10.3390/su141912833

Academic Editors: Javier Orozco-Messana and Martijn Rietbergen

Received: 13 August 2022
Accepted: 7 October 2022
Published: 8 October 2022



## 1. Introduction

Low-temperature radiant floor systems comprise the following components from top to bottom: surface layer, filling layer, insulation layer, and floor. The insulation layer prevents the transfer of heat downstairs, and the choice of surface material affects the surface heat distribution of the floor [1]. This construction mode has been widely used in buildings since it enables the floor to exhibit excellent thermal physical properties, while providing the [2] advantages of a small indoor vertical temperature difference, stable indoor thermal environment, and satisfying human thermal comfort. During the operation of the floor heating system, the floor can store heat throughout the structure, thus leading to a heat gain effect. However, the floor must be built using a material with heat storage ability, such as concrete and cement. Different concrete materials have varying thermal hysteresis characteristics; thus, the heat storage performance of the floor differs. Accordingly, [3,4] the thermal physical properties of the internal materials of a floor have an important influence on the heat storage ability of the floor. The change to a modern life style has increased [5] the heating demands of households at night, with intermittent heating becoming an inevitable trend [6,7]. According to the periodicity of sunshine, solar energy is used in the winter for heating purposes and meets the heating demand of households while saving energy. Therefore, it is necessary to study the floor heat storage performance to make full use of the solar energy resources and meet the intermittent heating needs of households.

Previous studies have primarily been based on either the system operation control strategy or the floor thermal performance. Nevertheless, the fundamental purpose of

both these types of studies is to improve the low-temperature radiant floor system to ensure indoor thermal comfort and reduce energy consumption. To study the control strategy of systems influenced by factors such as site and environment, most studies establish prediction models. Zhang [8] developed a simplified dynamic thermal network model and a state space model based on various thermal physical parameters, and the simulated values showed an error of less than 7% when compared to the measured values. Wang [9] successfully used a state space model and genetic algorithm to estimate the thermal physical parameters. However, due to a large thermal inertia of the concrete on the floor, there is a lag in the response of indoor air temperatures. The traditional control model rarely compensates for the thermal hysteresis of the concrete on the floor and does not have the capability to produce a spatial thermal response in time [10]. Several studies have applied model predictive control (MPC) schemes in building environments [11]. MPC integrates prediction, parameter optimization, and feedback control, while reducing the energy demand during peak hours by compensating for the thermal mass of the building [12]. In studies elucidating the floor thermal performance, materials with good heat storage performance are often used for experiments and simulations (such as phase change materials) to balance energy consumption and user demand. Meanwhile, new materials obtained by combining phase change materials with traditional building materials can greatly improve the heat storage capacity of buildings [13]. Guo et al. [14] considered the thermal capacity of phase change materials under solar radiation and found that solar radiation can increase the indoor temperature by more than 3 °C. Suna et al. [15] constructed a phase change floor with a thermal storage layer and cold storage layer, and they found that the thermal comfort time in the winter was twice that observed in ordinary rooms. Although phase change materials can greatly improve the thermal inertia of buildings [16], the high melting point of phase change materials is not suitable for use in the room temperature environment of the building, and the stiffness of the support material is high [17]. Besides, improper operations in the use process can easily fracture the support material, resulting in the leakage of the phase change material. From the perspective of studying the thermal properties of the floor, this study summarizes the problems of phase change materials. Since materials with strong thermal stability and high thermal inertia should be selected, this study utilizes concrete as the heat storage material of the floor heating model. Previous research [18] has explored the variation in the indoor thermal environment, floor heating, or the influence of solar radiation [19]. Furthermore, the heat transfer efficiency of concrete comprising steel powders under the heat transfer condition has also been discussed [20]. However, a low-temperature radiant floor has never been used as a thermal energy storage system. Moreover, a systematic design of floor heat storages made of concrete has not been developed; thus, quantitative research on the capacity of floor heat storages is required, and the systematic design of concrete heat storage materials needs to be further investigated.

Thermal energy storage system (TES) represents the heat storage mode of concrete materials. There are three types of TESs, namely: sensible heat storage (SHTES), latent heat storage (LHTES), and chemical heat storage (TCS). When low-temperature radiant floor pipes are heated, hot water can generate forced convections [21,22] under pressure in the tube. Meanwhile, a heat transfer occurs between the hot water and pipe wall, and the heat is further transferred via conduction and convection to a heat storage material. This phenomenon is based on SHTES [23] and does not alter the phase state; however, it changes the temperature. When concrete temperature rises, energy content increases. After the heating stops, stored heat is released from the material and transferred to regions with lower temperatures. Moreover, the stability of the indoor thermal environment is maintained through the convection and radiation heat exchange with air. SHTESs can balance the supply and demand of energy and have the potential to increase the energy conversion efficiency of the equipment. The factors related to the SHTES materials include thermal conductivity coefficient, thermal diffusion coefficient, specific heat capacity, heat loss, and volume heat capacity. However, the SHTES capacity of a material depends more

on its energy density (that is, the heat capacity per unit volume) [24]. As the heat storage mode of the floor involves fluid heat transfer in the pipe, convection heat transfer between the pipe and heat storage material, and heat conduction in the heat storage material, it is not easy to select the appropriate SHTES material. Generally, the heat energy formula associated with SHTES is [25]:

$$Q = cslo \cdot \rho slo \cdot Vslo \cdot \Delta T \quad (1)$$

where Q is the heat in J, cslo is the specific heat capacity of SHTES in J/(kg·K), ρslo is the density of SHTES in kg/m$^3$, Vslo is the volume of SHTES, and ΔT si the material surface temperature difference in °C.

To correctly design a heat storage system, the dynamic behavior of heat transfer over time should be considered in the heat storage process. However, the above-mentioned formula does not consider the change in time. Thus, Ferone et al. modified the formula, as follows [26]:

$$Qeff = \rho sol \cdot Vsol \cdot csol \cdot \Delta Teff \quad (2)$$

where Qeff represents the effective heat that can be stored by SHTES via dynamic circulation heat storage, and ΔTeff is the temperature difference of the material surface over time in °C.

When a floor is used as a TES, the thermophysical phenomena of the floor are generally studied using the finite element analysis method (FEM) [27–30]. This method can solve complex problems by treating them as domain objects that are divided into finite element interconnect subdomains, after which the approximate solution of each unit is simplified; subsequently, the approximate solution of the domain is determined. FEM is applied in practical engineering, since it is one of the most efficient numerical methods to solve transient heat transfer problems. To elucidate the behavior characteristics of concrete materials, the model established in this study ignores the non-uniform structure of concrete components and transforms them into homogeneous materials.

Concrete materials are an important part of the floor heat storage system, which were originally designed for architectural applications. Owing to their varying composition, the thermal and mechanical properties of concrete materials demonstrate diversified performance. They have also been widely used for industrial waste heat recovery in power plants [31,32]. In addition [33], TESs have been used to store the industrial waste heat to improve its utilization rate. Thus far, the research on concrete has increased its recyclability, greenness, and durability. For example, the physical properties of plastic wastes have been changed using chemical treatment or via their addition into concrete as aggregates. Some studies have proved that the compressive strength of concrete produced by this method reaches [34] MPa19. The choice of aggregate has evolved from natural ores to industrial and agricultural wastes, [35] such as construction demolition waste and agricultural waste, including coconut shells. Concrete with ground-granulated blast furnace slag exhibits more reliable thermodynamic properties than traditional concrete; thus, it can be used for heat storage. The study has revealed that adding straw fiber concrete to concrete with blast furnace slag improves physical properties [36,37]. In addition, the heat storage performance of concrete SHTESs is determined by studying the energy consumption of buildings [38]. An overview of the design method used for concrete SHTESs is shown in Figure 1.

The above-mentioned literature reveals that it is necessary to study floor heat storage for the following reasons: First, although concrete SHTESs are common, most studies only consider the heat storage of concrete from the perspective of thermal performance of concrete modules, and do not put it into practical application. Therefore, concrete SHTESs are combined with a low-temperature radiant floor; it is valuable to study the actual operation of this process. In addition, the thermal physical properties of concrete materials are used to study their thermal behavior from an intermediate perspective; however, there is still scope to achieve a better understanding by studying the heat storage behavior of concrete from an intermediate perspective. Finally, due to the complex thermal behavior of concrete SHTESs, few studies have analyzed the dynamic heat storage rate and

specific heat storage of concrete. By simplifying the complexity of simulation, the above problems can be effectively solved. Therefore, this study considers the thermal physical properties of concrete materials in the filled layer from an intermediate perspective, takes concrete SHTES as the research object, and uses the finite element method to conduct the numerical simulation of the transient behavior of heat storage in the floor by sorting out the thermal characteristics of different types of common concrete materials in literature. Furthermore, this study analyzes the dynamic thermal process of a low-temperature radiant floor, elucidates the heat storage characteristics of different types of concrete floors and the influence of material thermal physical properties on the heat storage of floors, determines the correlation between the heat storage of concrete floor with its influencing factors, and provides a reference for selecting internal structural materials that can be used in low-temperature radiant floors.

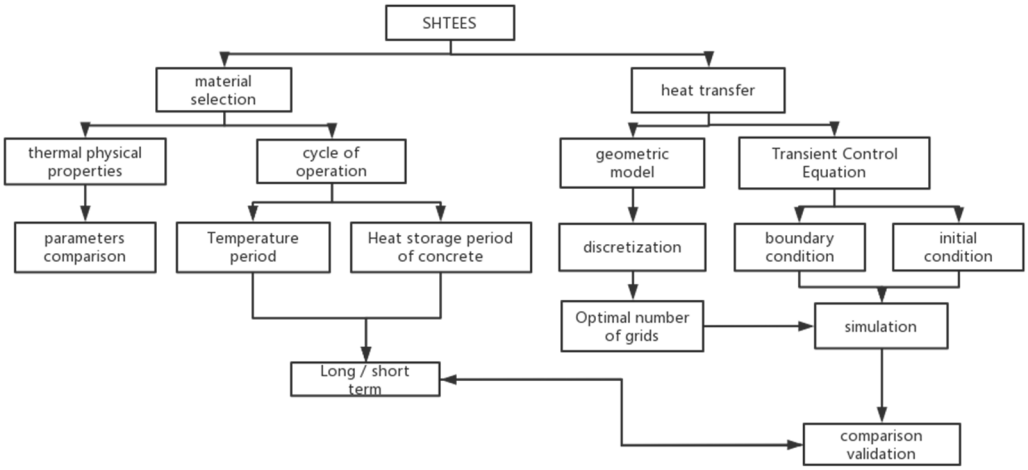


**Figure 1.** Design method of the SHTES system for concrete materials.

## 2. Materials and Methods

### *2.1. Governing Equation*

The primary equation used in this study is based on the basic principle of Ansys computational fluid dynamics (CFD) simulation. By considering the heat transfer of concrete and situation of the floor, the energy equation of concrete in the heating process can be written. The purpose of this equation is to express the energy conservation relation in the computational domain and obtain the temperature field in this domain. To simplify the calculation, radiation heat transfer has not been not considered. When the physical property parameters of the material are constant, the following formula is adopted [39]:

$$\frac{\partial T}{\partial t} + \nabla(UT) = \alpha \nabla^2 T \tag{3}$$

When the floor is being heated, the heat storage capacity and heat storage rate change with time. When the temperature of the floor surface becomes stable, the heat storage at each point inside the floor differs. Meanwhile, concrete SHTESs store heat by altering their surface temperatures without changing their phase. Therefore, the filling layer material is taken as the variable in heat storage research to analyze the total heat storage of the floor and the instantaneous heat storage rate at different positions.

In the process of heat storage, the instantaneous heat storage rate at a particular time and position is equal to the slope of the instantaneous heat storage; here, the instantaneous heat storage is the difference between the heat dissipation on the contact surface of the coil and the filling layer and the heat dissipation on the floor surface and the coil surface during the heating period [40]:

$$q_p = \int_s q_2 ds, \quad q_f = \int_0^1 q_1 dx \tag{4}$$

$$q_c = q_p - q_f = \left[ \int_0^1 q_1 dx - \int_s q_2 ds \right] \quad (5)$$

where q1 is the heat flow distribution law of the floor surface ($W/m^2$), $q_2$ is the coil surface at a certain time during heating period ($W/m^2$), s represents the semi-arc length of the radiant floor coil (m), $q_f$ is the instantaneous heat loss from the floor surface (W), and $q_c$ is the instantaneous heat storage of the floor during heating (W). By fitting and analyzing the instantaneous heat storage, the mathematical fitting expression is obtained and the total heat storage of the floor is determined.

### *2.2. Design and Simulation Method Used for the SHTES Floor*

The floor model has been designed to calculate the energy transfer and absorption of concrete over time. Thus, a plate length of one meter in parallel tube direction and a plate width of two tubes in vertical tube direction is a calculation unit. The cell can be regarded as a symmetric repeating unit that can form the entire floor, with its characteristic pipe line spacing (lh) and plate thickness. Figure 2 shows a schematic of the floor unit.

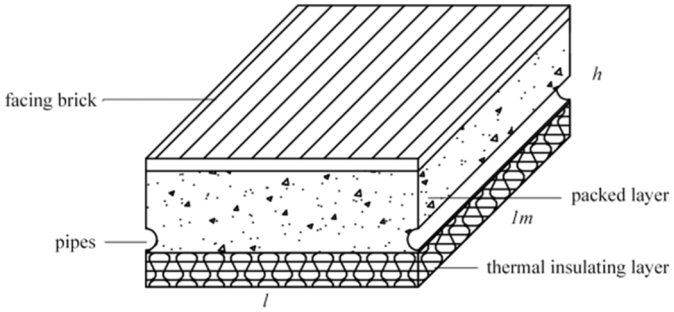


**Figure 2.** Schematic of the floor unit.

To ensure that the solution lies within the surface and boundary conditions and to reduce the number of computer calculations, a structured grid has been adopted (Figure 3). The standard grid independence test, which is the standard procedure for numerical simulations, shows that increasing the number of grid cells after reaching a certain level has no effect on the calculation result [41]. The models have a size of 200 mm × 67 mm. The shortest edge is selected as the basis of grid division, while four different kinds of grids with varying densities are chosen. The number of cells in grids named A–D is 77,592, 1,218,978, 2,035,352, and 3,386,304, respectively. Furthermore, grids exhibit good quality, which indicates that the grid division is reasonable. Figure 4 shows that the variations in floor surface temperatures in the four grids gradually decrease after the number of grid cells reaches 2,035,352; thus, grid C is selected to save costs.

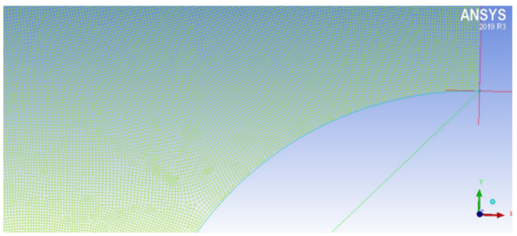


**Figure 3.** Node graph of the computing domain.

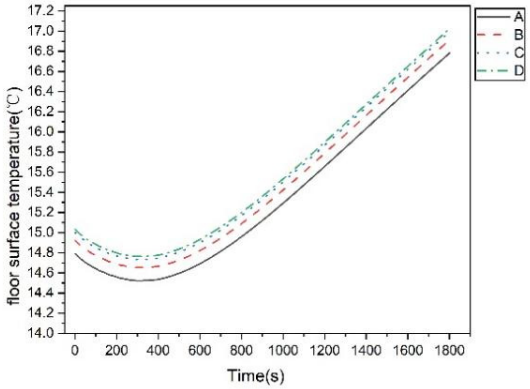


**Figure 4.** Grid independence verification.

The thermal analysis of the internal floor unit can be summarized as the study of the heat transfer phenomenon of the filling layer in the floor, which is used as the unit for storing heat. This method of dividing units has been adopted in many studies [42]. The advantage of this approach is that the minimum differential of the storage unit can be described, and that the grid computing domain can be divided easily via numerical simulation. Since floor heat storage changes with time, an unsteady heat transfer mathematical model has been adopted in this study. In the numerical simulation of unsteady heat transfer [43,44], the complexity of model simulation can be reduced through various published methods. In this study, the two-dimensional floor model has been adopted as the physical model.

The control accuracy of the model solution is at most 20 iterations in each step, the time step is 5 s, and the number of time steps is 360. The residual monitor was set to obtain the curves for floor surface temperature and heat flow change over time in a transient simulation environment, and the dynamic monitoring windows were set for the heat flow densities of different floor sections. The results were required to output heat flow density curves and other data acquired at the monitoring points inside the floor (Figure 5). The boundary conditions of this unsteady model are complex and difficult to solve. Therefore, the model has been further simplified based on the literature [8,9,12]:

1. The coil material used here is high-temperature resistant polyethylene (PE-RT) with good thermal conductivity; it can ignore the heat transfer effect of the coil on the filling layer. Accordingly, the temperature of the contact surface between the filling layer and the tube wall can be similar to the temperature of the outer surface of the tube wall;
2. The material of each layer is uniform and isotropic;
3. The water flow rate in the coils is high, and the temperature drop along the flow direction of the pipeline can be ignored. Since it is a two-dimensional heat conduction model, the heat is transferred along the thickness of the floor in a direction between the adjacent coils.
4. When designing a floor structure, the interlayer formed between the coil and insulation layer is generally set using a reflection film; this leads to excellent prevention of heat loss because the bottom of the coil and floor surface function as the adiabatic boundary and heat dissipation boundary, respectively.

The heat storage process of the SHTES module can be expressed using a thermal conductivity differential equation in which the thermal conductivity coefficient is regarded as a constant [45]:

$$\frac{\partial t}{\partial \tau} = \alpha\left(\frac{\partial^2 t}{\partial x^2} + \frac{\partial^2 t}{\partial y^2}\right) \quad (6)$$

Boundary and initial conditions determine the storage period and upper limit of the SHTES module. The fixed solution conditions are as follows: since the temperature field of each unit of floor has symmetry, the bottom surface parallel to x axis and the two sections

parallel to y axis of the model are set as the adiabatic boundary, namely: x = L /2, x = −L /2, and Y = 0:

$$\left.\frac{\partial t}{\partial x}\right|_{x=l/2,x=-l/2} = 0 \quad (7)$$

$$\left.\frac{\partial t}{\partial y}\right|_{y=0} = 0 \quad (8)$$

For floor radiant heating, the surface heat transfer coefficient (Hz) and indoor ambient temperature (t0) are defined as known conditions; thus, a third type of boundary conditions is adopted [46]:

$$\lambda\frac{\partial t}{\partial y} = h_z(t - t_0) \quad (9)$$

where α represents the thermal diffusivity ($m^2/s$), L is the coil spacing (mm); X and Y are the horizontal and vertical coordinates of the floor structure, respectively; $h_z$ denotes the comprehensive heat transfer coefficient of the floor surface ($W/(m^2 \cdot °C)$); t and $t_0$ are the floor surface temperature and indoor environmental temperature, respectively (°C); and Tau represents time.

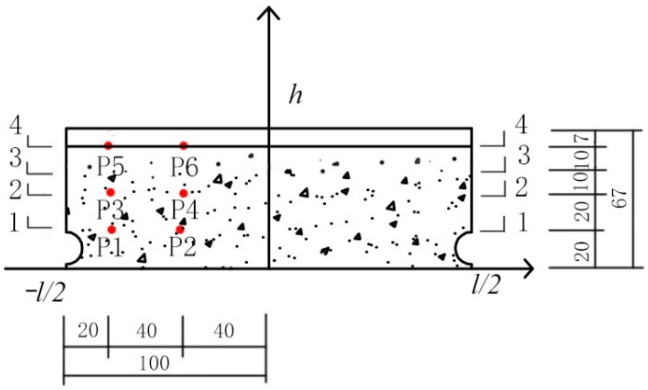


**Figure 5.** Floor physical model and measuring point positions (units mm).

The initial conditions of the floor surface are t = 15 °C and τ = 0, and the width of the floor is 1 m. Under the initial condition, the indoor temperature is 15 °C, and the heat exchange between the floor and the environment includes convection heat transfer and radiation heat transfer. Therefore, the comprehensive heat transfer coefficient of the floor surface considering convection and radiation is set at $h_z$ = 10.5 W ($/m^2 \cdot °C$), as shown in Table 1. After a temperature load is applied, to minimize computer operations, the heat storage process within half an hour from the initial state of the floor is determined, and the temperature field within half an hour after heat storage is obtained.

**Table 1.** Initial conditions of floor operation.

| Coil Heating Temperature °C | Coil Spacing mm | Initial Temperature °C | Comprehensive Heat Transfer Coefficient W(/$m^2 \cdot °C$) |
|---|---|---|---|
| 42 | 200 | 15 | 10.5 |

### *2.3. Screening Concrete SHTES Materials*

Concrete is a filling material with significantly large volume heat capacity; this study [47–49] selected literature and books related to several kinds of commonly used concrete materials. Consequently, a few concrete groups, which comprise clay ceramic (aggregate) and an admixture (fly ash and blast furnace slag powder), are suitable for a low-temperature radiant floor. The specific thermal parameters are shown in Table 2, where FAC represents concrete with pulverized coal ash, SC represents slag concrete, and

CAC represents concrete with clay ceramic. The water content at the initial stage affects the specific heat capacity of concrete, which in turn plays a key role in the heat storage capacity of concrete [50]. However, this study only elucidates the influence of thermal and physical parameters on heat storage. Nevertheless, to reduce the influence of specific heat capacity on the concrete storage and simplify the simulation, the specific heat capacity is kept constant.

**Table 2.** Thermal physical performance of concrete.

| Name | Thermal Conductivity W(m·K) | Specific Heat Capacity J/(kg·K) | Density kg/m$^3$ | Thermal Diffusivity m$^2$/s | Volumetric Heat CapacitykJ/(m$^3$·K) |
|---|---|---|---|---|---|
| FAC1 | 0.95 | 1050 | 1700 | $5.32 \times 10^{-7}$ | 1785 |
| FAC2 | 0.7 | 1050 | 1500 | $4.44 \times 10^{-7}$ | 1575 |
| SC | 1 | 1050 | 1700 | $5.6 \times 10^{-7}$ | 1785 |
| CAC1 | 0.7 | 1050 | 1400 | $4.76 \times 10^{-7}$ | 1470 |
| CAC2 | 0.84 | 1050 | 1600 | $5 \times 10^{-7}$ | 1680 |

The concrete types mentioned above are first selected based on specific heat capacity and volume heat capacity [51]. Because high-volume heat capacity directly determines the degree of the heat storage per unit concrete, the specific heat capacity reflects its thermal inertia. Meanwhile, the types of aggregate and cement used are key factors affecting the thermal characteristics. The higher the water-cement ratio of cement, the greater the number of voids in concrete; these voids reduce the thermal conductivity and specific heat capacity of concrete. Different aggregates exhibit distinct thermal conductivity, and the proportions of coarse and fine aggregates have an important influence on the thermal characteristics of concrete. Moreover, considering the low-carbon green effect, utilizing slag concrete can effectively inhibit the hydration heat of cement and reduce the generation of $CO_2$ by maintaining the high strength of concrete. As for the current research progress of materials selected in this study, [52] most of them are either mixed with admixtures to improve the thermal physical properties of concrete or with phase change materials (PCM) to improve the heat storage capacity of concrete; this improves the applicability of various materials used in construction [53,54].

The thermophysical performance indexes of concrete SHTES capacity include the specific heat capacity, volume heat capacity, and thermal diffusion coefficient; here, the heat capacity refers to the heat storage capacity per unit volume. Meanwhile, the specific heat capacity refers to the heat storage capacity per unit mass of the material; that is, the quantity of heat absorbed per unit mass of the material when its temperature increases by 1 °C. It is calculated using the following formula: Cρ. C refers to the relationship between the heat energy and temperature performance of the material per unit volume. The thermal diffusivity α (calculated using k/Cρ) represents the rate of the diffusion of heat through the material. According to the above-mentioned material selection and literature research, some conclusions can be drawn:

1. Heat transfer within a concrete material mainly occurs via heat conduction, and the factors affecting thermal conductivity are aggregate type, water-cement ratio, and moisture content. In addition, the influence of thermal conductivity on thermal performance is also related to temperature. When the concrete temperature rises, its thermal conductivity is significantly reduced; however, this effect is only observed when the temperature exceeds 500 °C [55].
2. Volumetric heat capacity is an important factor affecting the temperature distribution inside concrete. It decreases rapidly with a decrease in water content at the initial stage. Therefore, compared with the ideal situation of a constant volumetric heat capacity, the volumetric heat capacity is altered with environmental changes [56].

3. The selection of concrete as a heat storage material should be based on the selection of materials with high thermal performance. It should be ensured that the SHTES module maximizes heat storage benefits.
4. The thermal diffusion coefficient should be appropriately increased, since the concrete mix design can significantly affect the thermal characteristics [57].

The above discussion proves that the concrete material selected in this paper has a high thermal diffusion coefficient and volume heat capacity. Therefore, the data in Table 2 can be used as a reference for simulation. To ensure that the variables remain consistent, the other materials of floor construction use the same standard.

## 3. Results

### *3.1. Changes in Floor Temperature and Heat Flux*

After simulating the working conditions of the five concrete filling layers, the floor surface temperature diagram after 30 min loading was obtained (Figure 6). In 200 s, the temperature shows a linear drop as the floor surface heat diffuses to the indoor environment. After 200 s, the temperature change curve becomes exponential. After 30 min of heating, the surface temperature of each concrete material differed according to its thermal performance. The floor surface temperatures are 16.9921°C, 15.7441°C, 18.0665°C, 15.8532°C, and 16.6585°C. In the case of constant coil temperature, the curve of the floor surface temperature with time indicates the heat gain capacity of concrete material inside the floor, and a steeper curve indicates that the material is sensitive to temperature change.

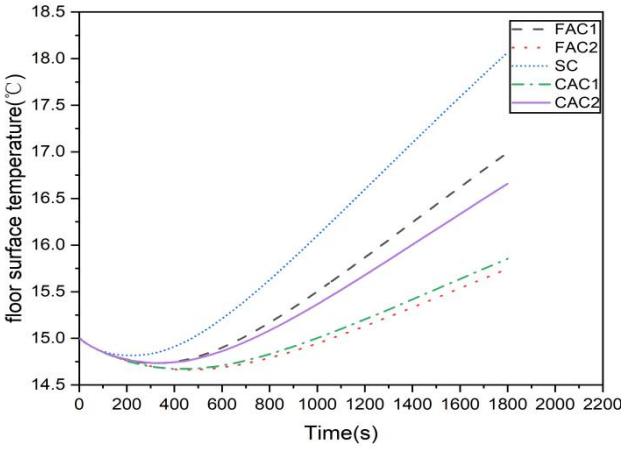


**Figure 6.** Radiant floor temperature rate.

Figure 7 shows the distribution density of the internal floor temperatures for the five concrete materials, which was determined using a simulation based on the physical model and measuring points shown in Figure 5. The results at different measuring points were simulated to form a dataset by using distribution density plots of time and temperature that represent various types of concrete materials. Density plots show that the peak location of the temperature distribution within the time period is the most concentrated. When the coil temperature becomes constant, the heat stored in concrete per unit volume increases by one degree and the temperature inside the floor rises faster. The figure shows that the temperature mostly fluctuates between 14 °C and 16 °C. This is because the initial temperature of the floor is 15 °C and the concrete material has the characteristics of a temperature wave attenuation at the initial heating stage, resulting in a slow temperature rise rate. The temperature distribution of SC and FAC1 is uniform, with temperature ranging from 15 °C to 18 °C; this indicates that the amount of heat absorbed increases and the temperature changes quickly under these two working conditions.

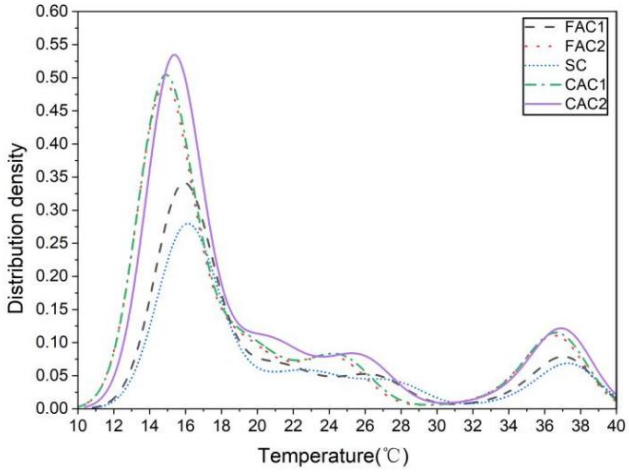


**Figure 7.** Temperature distribution of the internal floor unit.

To reduce the influence of uneven temperature, the heat storage capacity of concrete materials has been evaluated by utilizing the average temperature values in addition to the distribution density analysis. Figure 8 shows the boxplots of the internal floor temperatures for the five kinds of concrete materials. The beard line in the figure represents the standard deviation, the line in the box plot represents the average value, and the curve on the right is the normal distribution curve of discrete points. It can be found from the discrete data points that the data dispersion is large between 25 °C and 30 °C, and that the reason for the formation of both ends of temperature is closely related to the heating time. Therefore, the average values were used to reduce the inhomogeneity of temperature distribution. The average values of each group were between 20 °C and 22 °C, and the highest values of FAC1 and SC groups were 21.02 °C and 21.52 °C, respectively. However, the large standard deviation indicates that the data points are significantly different from the average value at this time; thus, the further analysis of concrete heat storage is needed.

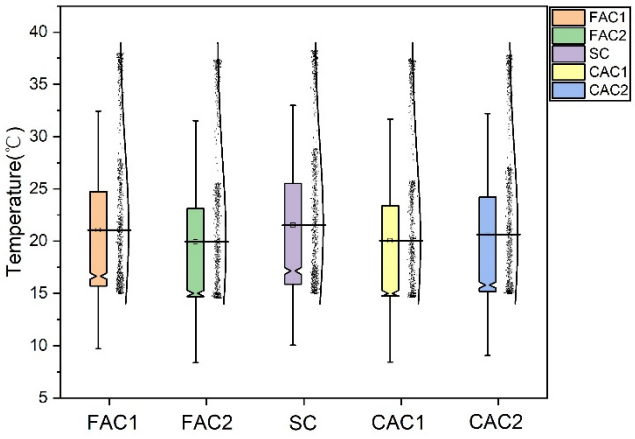


**Figure 8.** Box diagram representing the temperature of the internal floor unit.

Figure 9 shows the internal temperature map of the floor after heating for 30 min, which highlights the static temperature field inside the floor. The scale on the left represents the accuracy of the temperature with the help of various colors. As the temperature inside the floor (shown in the picture) is in the early stage of heating, the temperature mostly lies in the blue part of the scale (15.3 °C to 18 °C). The uneven temperature distribution can reduce the heat storage efficiency of concrete materials. The temperatures associated with FAC2 and CAC1 generally lie in the dark blue part of the scale, while those associated with SC rarely lie in the dark blue part. In this stage, the SC floor exhibits a high heat transfer efficiency and rapid temperature change.

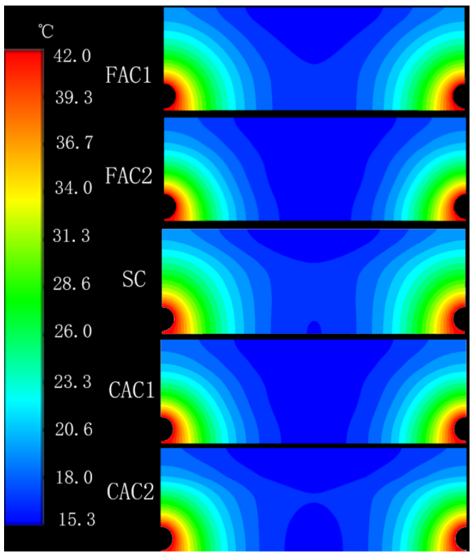


**Figure 9.** Static temperature field inside the floor after 30 min.

In the heating process of the floor, the change rule of heat flux in each layer is closely related to the distance between the coils and positions on the floor. The heat flux in each section of the floor at the initial heating stage is shown in Figure 10. The closer the section is to the coil, the faster the heat flow density changes per unit time. Therefore, the heat flow density curve in Figure 10a is steep within 200 s; however, the change rate of heat flow density slows down after 200 s, and the heat from the coil is transferred to Section 1. Figure 10b shows that heat flow density changes greatly within 400 s. At this time, the heat inflow rate in Section 2 is high, and a relatively stable curve appears after 400 s. The curves in Figure 10c,d exhibit similar changes, indicating that the heat transfer rate to the floor surface is slow at the initial heating stage. Therefore, the thermal physical properties of different concrete filling layers have a great influence on the heating of sections at different positions between the floor and the coil at the initial heating stage.

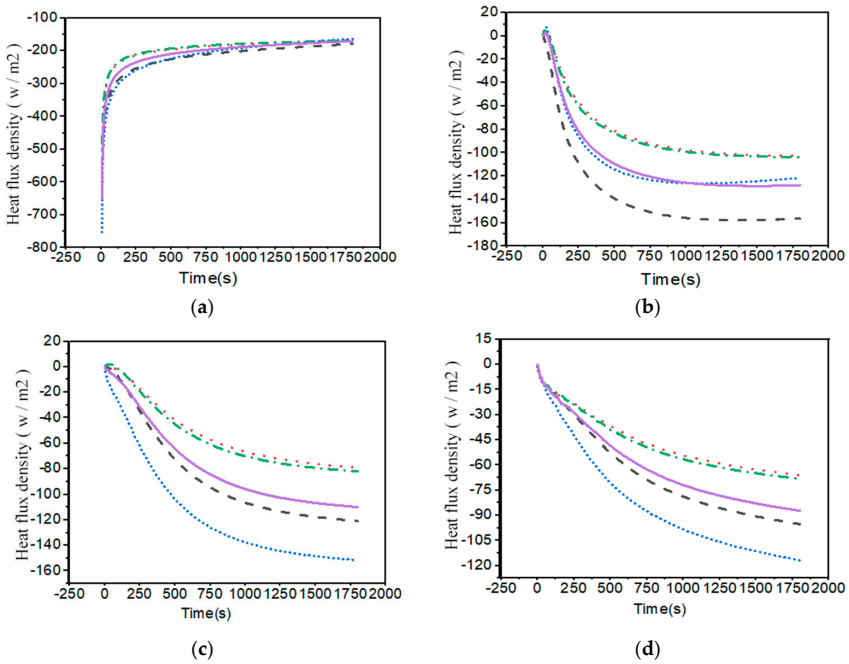


**Figure 10.** Heat flux density of the floor in different sections: (**a**) section 1 (at 20 mm), (**b**) section 2 (at 40 mm), (**c**) section 3 (at 50 mm), and (**d**) section 4 (at 60 mm).

### *3.2. Influence of Concrete Thermal Properties on Heat Storage Process*

Analysis of the simulation results of temperature and heat flux reveals that the thermal physical properties of concrete have a significant influence on the heat storage process of the floor. According to Table 2, concrete materials with a larger volume heat capacity exhibit higher thermal conductivity, indicating that an increase in thermal conductivity can enhance the heat storage capacity per unit volume. When two groups of materials exhibit the same thermal conductivity and specific heat capacity, the volume heat capacity is affected by density. The higher the density, the higher the volume heat capacity, and the stronger the heat storage capacity. In addition, when the volume heat capacity and density are the same, the influence of the thermal conductivity of concrete material on the heat storage capacity needs to be analyzed in detail.

To study the influence of thermal conductivity on heat storage capacity, a dataset with different thermal conductivities and other variables has been selected for analysis; FAC1 and SC are used to analyze the floor surface temperature and floor surface heat flow (Figure 11). After the floor system started its operation, the heat flow and temperature of the floor surface exhibit an opposite trend, indicating that the direction of heat flow is opposite to the direction of temperature gradient for isotropic materials. The figure defines heat inflow as negative and heat outflow as positive. SC exhibits a high thermal conductivity, and the temperature and heat flow of the floor surface change quickly. However, the heat outflow from the floor surface of FAC1 reached its peak before 500 s, indicating that the heat transfer rate of the FAC1 floor interior was lower compared to that of the SC floor interior in the same period of time; therefore, heat did not transfer to the floor surface. At this time, the temperature of the FAC1 floor surface dropped rapidly. After 500 s, the temperature of the FAC1 floor surface rises gradually and the heat flow into the floor surface increases, indicating that the internal heat is transferred to the floor surface only after more heat is absorbed inside the floor. Because this coefficient of thermal conductivity is smaller, the quantity of the heat that passes inside the unit time is less; thus, the quantity of heat transferred to the floor surface is minimal.

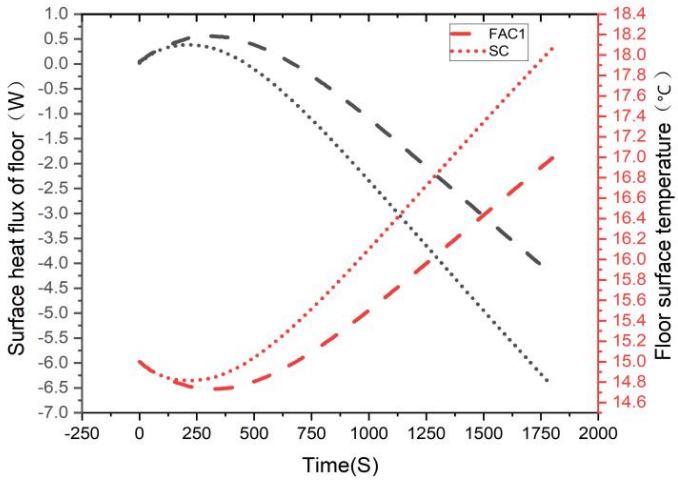


**Figure 11.** Heat flux, time, and temperature of FAC1 and SC floor surfaces.

The above analysis demonstrates that a lower thermal conductivity renders heat storage more unfavorable. However, the thermal diffusion coefficient of concrete also affects the actual heat storage of the floor. According to the thermal diffusivity of the concrete calculated in Table 2, the thermal diffusivity exhibits the following decreasing order: SC, FAC1, CAC2, CAC1, and FAC2. From the theoretical perspective of heat storage, the smaller the thermal diffusion coefficient, the lower the rate of heat diffusion through the material itself; that is, the heat is maintained for a certain period of time without external diffusion, which is not conducive to the absorption of heat in concrete materials. From a practical point of view, floor heating is closely related to the indoor thermal environment

and human comfort. A larger thermal diffusivity increases the absorption of heat inside the floor and facilitates the escape of heat to the outdoor environment, which affects the indoor temperature response. Therefore, the influence of thermal diffusivity on the indoor thermal environment should be controlled.

## 4. Discussion

Through the review of floor heating and the comprehensive analysis of results, it can be concluded that concrete materials with different aggregates and admixtures have a great impact on the floor heating capacity; this has also been confirmed by Wang et al. [58]. In general, SC and FAC1 are more suitable for floor heating. To determine the influence of low-temperature radiant floor building on indoor thermal environment, Li et al. [59] designed a movable modular radiant board to study its influence on the indoor thermal environment; they found that the indoor temperature can be kept at 21 °C, which has a good effect on maintaining the indoor thermal environment. If a concrete floor and solar energy are used together, energy can be saved and the indoor thermal comfort can be significantly improved.

Based on the floor surface temperature, a comparative analysis has been conducted with related literature in this study. Table 3 lists the floors similar to those used in this study through literature sorting, and the analysis results are shown in Figure 12. As can be observed from the figure, the simulation results exhibit the same general trend that is observed in the literature sorting results. After 900 s, both the datasets show an increasing trend with an increase in heating time; the average difference in floor surface temperature is 0.57 °C, and the maximum difference in plate temperature is 1.8 °C. The literature data are higher than the simulation data in this study. Although the heating temperature and initial temperature of the coil in the literature are slightly lower than that in this study, the coil spacing is half of that in this study, indicating that the floor heating rate increases with a decrease in the coil spacing. Therefore, the error between the results of the simulation method and the results of literature sorting is less than 5%, which can be regarded as accurate.

**Table 3.** Data from literature.

| Coil Heating Temperature °C | Coil Spacing mm | Initial Temperature °C | Literature Resource |
|---|---|---|---|
| 40 | 100 | 14 | [50] |

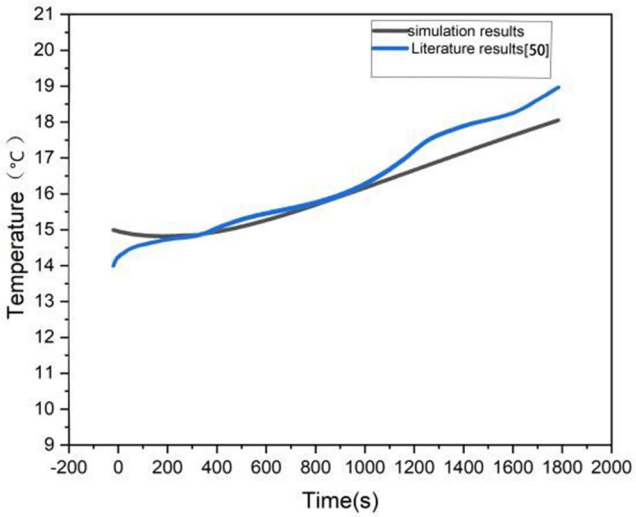


**Figure 12.** Comparison of simulation and literature results.

### *4.1. Floor Heat Storage*

The instantaneous heat storage inside the floor can be calculated using the heat storage formula (Figure 13). The instantaneous heat storage exhibits the following descending order: SC, FAC1, CAC2, FAC2, and CAC1. As the heat storage capacity increases, temperature changes quickly; thus, the primary factor is the heat flux density of the floor surface. The simulation performance for heat flux density is better than that for the instantaneous heat flux. In addition, the working conditions of the heat storage under different periods and temperatures reflect the heat storage capacity of the floor, thus affecting the change in the instantaneous heat storage; a rise in the internal temperature of the floor increases the heat storage capacity, which leads to the complete heat absorption.

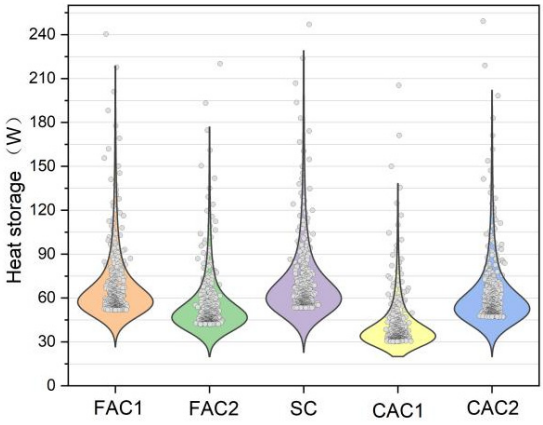


**Figure 13.** Instantaneous heat storage of the floor.

Working conditions are obtained using data fitting expressions, and the total heat storage is determined using an integral solution. Table 4 shows the capacity of the heat storage unit. In the existing literature, the fitting expression has been calculated within 0.5 h; however, for heater tubes, 7 h is an appropriate time to determine the fitting expression. Therefore, the heat storage can be predicted after 7 h using the expression. The total heat storage in most working conditions is within the range of 700–800 J, indicating that the overall heat storage is stable and that there is little difference between different working conditions. It is worth noting that the total heat storage of SC is the maximum (848.521 J) after 7 h, which verifies the results obtained through the analysis of heat flow density in the previous section. Therefore, the SC floor exhibits the best heat storage capacity.

**Table 4.** Total heat storage of the floor unit.

| Name | Fitting Expression | 0.5 h Total Heat Storage J | 7 h total Heat Storage J |
|---|---|---|---|
| FAC1 | $\int_0^m(-0.2154x+109.86)dx$ | 54.9031 | 763.743 |
| FAC2 | $\int_0^m(-0.1973x+94.265)dx$ | 47.1078 | 655.021 |
| SC | $\int_0^m(-0.2583x+122.12)dx$ | 61.0277 | 848.512 |
| CAC1 | $\int_0^m(-0.2005x+105.58)dx$ | 51.2075 | 702.038 |
| CAC2 | $\int_0^m(-0.2274x+107.59)dx$ | 53.7666 | 747.599 |

### *4.2. Instantaneous Heat Storage Rate inside the Floor*

Thermal change rate refers to the speed of heat absorption per unit area, which affects the heat storage rate. By calculating the slope of the curve plotting time and heat flow density and subsequent fitting, the thermal change rate under the cross-section of each layer is obtained.

Table 5 shows the instantaneous heat storage rate of sections in each layer inside the floor within half an hour after the heating period begins. The overall heat storage rate

decreases layer by layer, and the section close to the heating source has the fastest heat storage rate. The comprehensive heat storage rate is in accordance with the description of the floor heat storage. However, it is worth noting that the heat storage rate of the same section tends to change under different conditions. For example, there is a significant difference between the comprehensive heat storage rates of FAC2 and SC; however, the heat storage rate of FAC1 in Section 2 (0.20782 j/S) is significantly higher than that of SC, indicating that different concrete materials are applied to the low-temperature hot water radiant floor, and that the influence of their location on the maximum heat storage benefit should be considered.

**Table 5.** Instantaneous heat storage rate in the floor.

| Name | Section Location | Heat Storage Rate J/S | Comprehensive Heat Storage Rate J/S |
|---|---|---|---|
| FAC1 | Section1 | 0.38932 | 0.09469 |
| | Section2 | 0.20665 | |
| | Section3 | 0.26407 | |
| | Section4 | 0.24693 | |
| FAC1 | Section1 | 0.23293 | 0.09001 |
| | Section2 | 0.20782 | |
| | Section3 | 0.22346 | |
| | Section4 | 0.15443 | |
| SC | Section1 | 0.44923 | 0.09477 |
| | Section2 | 0.20238 | |
| | Section3 | 0.34339 | |
| | Section4 | 0.2742 | |
| CAC1 | Section1 | 0.22835 | 0.09314 |
| | Section2 | 0.20373 | |
| | Section3 | 0.22999 | |
| | Section4 | 0.20615 | |
| CAC2 | Section1 | 0.22094 | 0.09451 |
| | Section2 | 0.16703 | |
| | Section3 | 0.24527 | |
| | Section4 | 0.1867 | |

### *4.3. Correlation Analysis of Influencing Factors of Heat Storage*

The factors, which affect the instantaneous heat storage inside the floor, change the heat flow of the material that comes in direct contact with the heat source; this changes the heat flow on the floor surface as well as the heat storage rate of different positions inside the floor. To study the impact of these factors and instantaneous heat storage of the internal floor, a correlation analysis is necessary. The heat flow, temperature, and heat accumulation rate all exhibit a normal distribution; thus, the Spearman rank correlation coefficient (rs) can be determined by comparing the |rs| and significance ($p$) values. In general, $p$ values were significantly less than 0.05; when |rs| value is close to 1, the correlation is higher. Overall, |rs| is inversely proportional to the $p$ value; the effect of thermal storage on different working conditions is determined using a specific correlation analysis (Table 6).

The results of the correlation analysis demonstrate that the most relevant factors for instantaneous heat storage are the heat flow rate on the coil surface and heat storage rate inside the floor. When the floor is in use, the concrete material that improves the heat storage rate inside the floor can effectively increase the instantaneous heat storage. In addition, the floor surface temperature and heat storage demonstrated a strong negative correlation. This indicates that at the initial heating stage, the temperature wave of the internal floor exhibits an attenuation effect. The temperature drop rate of the floor surface affects its instantaneous heat storage; thus, the structural design of the floor surface at the initial heating stage can slow down the drop in surface temperature.

**Table 6.** Correlation analysis of factors influencing instantaneous heat storage in the floor.

| Name | Index | Spearman Rank Correlation Coefficient Rs | 0.05 Level of Visibility |
|---|---|---|---|
| FAC1 | Surface heat flux of coil | 1 | Obviously |
| | Floor surface temperature | −0.95421 | Obviously |
| | Heat storage rate in floor | 1 | Obviously |
| SC | Surface heat flux of coil | 1 | Obviously |
| | Floor surface temperature | −0.98577 | Obviously |
| | Heat storage rate in floor | 1 | Obviously |
| ACA2 | Surface heat flux of coil | 1 | Obviously |
| | Floor surface temperature | −0.94645 | Obviously |
| | Heat storage rate in floor | 1 | Obviously |

## 5. Conclusions

In this study, the thermal properties of concrete with different admixtures and aggregates were obtained by conducting a literature review and reading books. The following concrete materials were considered: ceramic concrete with pulverized coal ash (0.95 and 0.7 W/(m·K)), slag concrete (1 W/(m·K)), and concrete with clay ceramic (0.7 and 0.84 W/(m·K)). In CFD simulation, the applicability of different concretes to floor heat storages based on the SHTES design method was evaluated. Furthermore, the transient heat storage of concrete at the initial heating stage has also been considered. The following conclusions can be drawn from this study:

1. After the simulation of floor heating within half an hour, the analysis of the floor surface temperature and internal heat flux density shows that the results of different concrete types under the same conditions are quite different, among which SC is more suitable for floor heat storage.
2. Analysis of the thermal physical properties of concrete revealed that volume density and heat capacity exhibit same trends; the coefficient of thermal conductivity of floors comprising different concrete types had a greater influence on the heat accumulation; however, it is important to note that the heat storage material cannot be chosen based on a single thermal physical property, and that the heat transfer characteristics and thermal physical properties must be comprehensively considered.
3. The total heat storage capacity in slag concrete for 0.5 and 7 h has been determined via fitting and verification analysis (61.0277 and 848.512 J, respectively). Meanwhile, the heat storage rate in the floor is strongly correlated with the heat flow on the coil surface and the floor heat storage.

Concrete floors are widely used in modern buildings. This study provides a novel SHTES design method for the future development of a floor heat storage that can efficiently utilize solar energy. Although this study successfully simulates the heating process of different floors based on concrete SHTES, it is hindered by the short study periods and limited computational resources. Thus, longer periods of simulation need to be adopted. Furthermore, there is a need to refine the heat storage law. Since concrete SHTESs involve a variety of heat transfer lines, finite element simulation has been used to simplify the complexity of the study; however, this simplification leads to results that are approximate and not exact. Therefore, in future research, methods that can more closely simulate the actual situation must be used to obtain more accurate heat storage data for concrete by extending the simulation time span.

**Author Contributions:** This paper is the result of free, full, and equal collaboration among all authors. Y.W. is responsible for the computational simulation, field measurements, data compilation, and the writing of the first draft of the paper. G.X. conceived the paper and validated the methods, data, and conclusions. All authors have read and agreed to the published version of the manuscript.

**Funding:** This research was funded by the National Natural Science Foundation of China (grant no. 52168006), the significant science and technology subject of Inner Mongolia "The green building system integration optimization and engineering demonstration of grassland based on the cultural inheritance".

**Informed Consent Statement:** Informed consent was obtained from all subjects involved in the study. Written informed consent has been obtained from the patients to publish this paper.

**Data Availability Statement:** Not applicable.

**Conflicts of Interest:** The author declares no conflict of interest.

## References

1. Baek, S.; Kim, S. Determination of Optimum Hot-Water Temperatures for PCM Radiant Floor-Heating Systems Based on the Wet Construction Method. *Sustainability* **2018**, *10*, 4004. [CrossRef]
2. Yeom, G.; Jung, D.E.; Do, S.L. Improving a Heating Supply Water Temperature Control for Radiant Floor Heating Systems in Korean High-Rise Residential Buildings. *Sustainability* **2019**, *11*, 3926. [CrossRef]
3. Ying, X.; Li, W. Effect of Floor Shape Optimization on Energy Consumption for U-Shaped Office Buildings in the Hot-Summer and Cold-Winter Area of China. *Sustainability* **2020**, *12*, 2079. [CrossRef]
4. Li, Y.; Wang, D.; Li, S.; Gao, W. Impact Analysis of Urban Morphology on Residential District Heat Energy Demand and Microclimate Based on Field Measurement Data. *Sustainability* **2021**, *13*, 2070. [CrossRef]
5. Loibl, W.; Stollnberger, R.; Österreicher, D. Residential Heat Supply by Waste-Heat Re-Use: Sources, Supply Potential and Demand Coverage—A Case Study. *Sustainability* **2017**, *9*, 250. [CrossRef]
6. Kalder, J.; Annuk, A.; Allik, A.; Kokin, E. Increasing Solar Energy Usage for Dwelling Heating, Using Solar Collectors and Medium Sized Vacuum Insulated Storage Tank. *Energies* **2018**, *11*, 1832. [CrossRef]
7. Liu, Z.; Wu, D.; Jiang, M.; Yu, H.; Ma, W. Field Measurement and Evaluation of the Passive and Active Solar Heating Systems for Residential Building Based on the Qinghai-Tibetan Plateau Case. *Energies* **2017**, *10*, 1706. [CrossRef]
8. Wang, J.; Tang, C.Y.; Brambley, M.R.; Song, L. Predicting home thermal dynamics using a reduced-order model and automated real-time parameter estimation. *Energy Build.* **2019**, *198*, 305–317. [CrossRef]
9. Wang, Z.; Chen, Y.; Li, Y. Development of State space model for thermal dynamic analysis of buildings through model structure simplification. *Energy Build.* **2019**, *195*, 51–67. [CrossRef]
10. Chen, T. Application of adaptive predictive control to a floor heating system with a large thermal lag. *Energy Build.* **2002**, *34*, 45–51. [CrossRef]
11. Rawlings, J.B.; Patel, N.R.; Risbeck, M.J.; Maravelias, C.T.; Wenzel, M.J.; Turney, R.D. Economic MPC and real-time decision making with application to large-scale HVAC energy systems. *Comput. Chem. Eng.* **2018**, *114*, 89–98. [CrossRef]
12. Hu, M.; Xiao, F.; Jørgensen, J.B.; Li, R. Price-responsive model predictive control of floor heating systems for demand response using building thermal mass. *Appl. Therm. Eng.* **2019**, *153*, 316–329. [CrossRef]
13. Guo, J.; Jiang, Y.; Wang, Y.; Zou, B. Thermal storage and thermal management properties of a novel ventilated mortar block integrated with phase change material for floor heating: An experimental study. *Energy Convers. Manag.* **2020**, *205*, 112288. [CrossRef]
14. Guo, J.; Dong, J.; Wang, H.; Jiang, Y.; Tao, J. On-site measurement of the thermal performance of a novel ventilated thermal storage heating floor in a nearly zero energy building. *Build. Environ.* **2021**, *201*, 107993. [CrossRef]
15. Sun, W.; Zhang, Y.; Ling, Z.; Fang, X.; Zhang, Z. Experimental investigation on the thermal performance of double-layer PCM radiant floor system containing two types of inorganic composite PCMs. *Energy Build.* **2020**, *211*, 109806. [CrossRef]
16. Prieto, C.; Cabeza, L.F. Thermal energy storage (TES) with phase change materials (PCM) in solar power plants (CSP). Concept andplant performance. *Appl. Energy* **2019**, *254*, 113646. [CrossRef]
17. Jiang, Z.Y.; Qu, Z.G. Lithium–ion battery thermal management using heat pipe and phase change material during discharge–charge cycle: A comprehensive numerical study. *Appl. Energy* **2019**, *242*, 378–392. [CrossRef]
18. Oravec, J.; Šikula, O.; Krajčík, M.; Arıcı, M.; Mohapl, M. A comparative study on the applicability of six radiant floor, wall, and ceiling heating systems based on thermal performance analysis. *J. Build. Eng.* **2021**, *36*, 102133. [CrossRef]
19. Jara, E.R.; Ruiz-Pardo, Á.; García, M.C.; Ríos, J.A.T. Effect of Wood Properties and Building Construction on Thermal Performance of Radiant Floor Heating Worldwide. *Appl. Sci.* **2022**, *12*, 5427. [CrossRef]
20. Tota-Maharaj, K.; Adeleke, B.O. Thermal performance of radiant floor heating systems concrete slabs. *Proc. Inst. Civ. Eng. Energy* **2022**, 1–12. [CrossRef]
21. Abbas, N.; Shatanawi, W. Heat and Mass Transfer of Micropolar-Casson Nanofluid over Vertical Variable Stretching Riga Sheet. *Energies* **2022**, *15*, 4945. [CrossRef]
22. Abbas, N.; Shatanawi, W.; Abodayeh, K. Computational Analysis of MHD Nonlinear Radiation Casson Hybrid Nanofluid Flow at Vertical Stretching Sheet. *Symmetry* **2022**, *14*, 1494. [CrossRef]
23. Sarbu, I.; Sebarchievici, C. A Comprehensive Review of Thermal Energy Storage. *Sustainability* **2018**, *10*, 191. [CrossRef]

24. Fengwu, B.; Chao, X. Performance analysis of a two-stage thermal energy storage system using concrete and steam accumulator. *Appl. Therm. Eng.* **2011**, *31*, 2764–2771.
25. David, B.; George, C. *The Heat Equation*, 1st ed.; Chapman and Hall/CRC: Boca Raton, FL, USA, 1995.
26. Ferone, C.; Colangelo, F.; Frattini, D.; Roviello, G.; Cioffi, R.; Di Maggio, R. Finite element method modeling of sensible heat thermal energy storage with innovative concretes and comparative analysis with literature benchmarks. *Energies* **2014**, *7*, 5291–5316. [CrossRef]
27. Park, M.; Min, J.; Bae, J.; Ju, Y. Thermal Contact Conductance-Based Thermal Behavior Analytical Model for a Hybrid Floor at Elevated Temperatures. *Materials* **2014**, *13*, 4257. [CrossRef] [PubMed]
28. Wang, W.; Zeng, X.; Niyonzima, E.; Gao, Y.; Yang, Q.; Chen, S. Size Effect of Shear Strength of Recycled Concrete Beam without Web Reinforcement: Testing and Explicit Finite Element Simulation. *Sustainability* **2021**, *13*, 4294. [CrossRef]
29. Yu, B.; Hu, P.; Saputra, A.; Gu, Y. The scaled boundary finite element method based on the hybrid quadtree mesh for solving transient heat conduction problems. *Appl. Math. Model.* **2021**, *89*, 541–571. [CrossRef]
30. Lim, M.; Lee, C. A Study on the Heat and Stress Evaluation of Reinforced Concrete through High-Frequency Induction Heating System Using Finite Element Techniques. *Sustainability* **2021**, *13*, 6061. [CrossRef]
31. Hasan, A.; Al-Sallal, K.; Alnoman, H.; Rashid, Y.; Abdelbaqi, S. Effect of Phase Change Materials (PCMs) Integrated into a Concrete Block on Heat Gain Prevention in a Hot Climate. *Sustainability* **2016**, *8*, 1009. [CrossRef]
32. Selvam, R.; Castro, M. 3D FEM model to improve the heat transfer in concrete for thermal energy storage in solar power generation. *Energy Sustain.* **2010**, *43956*, 699–707.
33. Oti, J.; Kinuthia, J.; Adeleke, B. The Strength Characterisation of Concrete Made with Alumina Waste Filler. *Sustainability* **2020**, *12*, 10235. [CrossRef]
34. Del Rey Castillo, E.; Almesfer, N.; Saggi, O.; Ingham, J.M. Light-weight concrete with artificial aggregate manufactured from plastic waste. *Constr. Build. Mater.* **2020**, *265*, 120199. [CrossRef]
35. Chinnu, S.; Minnu, S.; Bahurudeen, A.; Senthilkumar, R. Recycling of industrial and agricultural wastes as alternative coarse aggregates: A step towards cleaner production of concrete. *Constr. Build. Mater.* **2021**, *287*, 123056. [CrossRef]
36. Ashour, T.; Morsy, M.; Korjenic, A.; Fischer, H.; Khalil, M.; Sesto, E.; Orabi, M.; Yehia, I. Engineering Parameters of Rice Straw Concrete with Granulated Blast Furnace Slag. *Energies* **2021**, *14*, 343. [CrossRef]
37. Hamad, M.A.; Nasr, M.; Shubbar, A.; Al-Khafaji, Z.; Al Masoodi, Z.; Al-Hashimi, O.; Kot, P.; Alkhaddar, R.; Hashim, K. Production of Ultra-High-Performance Concrete with Low Energy Consumption and Carbon Footprint Using Supplementary Cementitious Materials Instead of Silica Fume: A Review. *Energies* **2021**, *14*, 8291. [CrossRef]
38. Ozdenefe, M.; Dewsbury, J. Thermal performance of a typical residential Cyprus building with phase change materials. *Build. Serv. Eng. Res. Technol.* **2015**, *37*, 0143624415603004. [CrossRef]
39. Vijayan, P.K.; Nayak, A.K.; Kumar, N. Steady-state and transient analysis of supercritical natural circulation systems. In *Single-Phase, Two-Phase and Supercritical Natural Circulation Systems*; Woodhead Publishing: Sawston, UK, 2019; pp. 237–272.
40. Wang, D.; Liu, Y.; Wang, Y.; Liu, J. Numerical and experimental analysis of floor heat storage and release during an intermittent in-slab floor heating process. *J. Appl. Therm. Eng.* **2014**, *62*, 398–406. [CrossRef]
41. Yuanyuan, Z.; Mei, H.; Jiyuan, H.; Hou, R. CFD investigation for a 7-pin wire-wrapped fuel assembly with different shapes of fuel duct wall. *Ann. Nucl. Energy* **2020**, *141*, 107272.
42. Cho, J.; Park, B.; Lim, T. Experimental and numerical study on the application of low-temperature radiant floor heating system with capillary tube: Thermal performance analysis. *Appl. Therm. Eng.* **2019**, *163*, 114360. [CrossRef]
43. Weitzmann, P.; Kragh, J.; Roots, P.; Svendsen, S. Modelling floor heating systems using a validated two-dimensional ground-coupled numerical model. *J. Build. Environ.* **2005**, *40*, 153–163. [CrossRef]
44. Nering, K.; Stypula, K. Evaluation of Floating Floor System with Steady State Dynamics Simulation in the Context of Impact Sound Level. *IOP Conf. Ser. Mater. Sci. Eng.* **2019**, *471*, 062017. [CrossRef]
45. Dincer, I. Heat Transfer Aspects of Energy. In *Comprehensive Energy Systems*; Elsevier: Amsterdam, The Netherlands, 2018; pp. 422–477.
46. Erasmo, C.; Fiorenzo, A. *Solution of Sample Problems in Classical Thermoelasticity*; Academic Press: Cambridge, MA, USA, 2017; Chapter 2; pp. 25–80.
47. Wang, Y.; Zheng, T.; Zheng, X.; Liu, Y.; Darkwa, J.; Zhou, G. Thermo-mechanical and moisture absorption properties of fly ash-based lightweight geopolymer concrete reinforced by polypropylene fibers. *Constr. Build. Mater.* **2020**, *251*, 118960. [CrossRef]
48. Mizobuchi, T.; Ishizeki, K.; Sagawa, T.; Kanda, T. Study on the Influence of Minor Constituents in Blast Furnace Slag Rich Cement on the Thermal and Mechanical Properties of Concrete. *J. Adv. Concr. Technol.* **2019**, *17*, 46–61. [CrossRef]
49. Wadsö, L.; Karlsson, J.; Tammo, K. Thermal properties of concrete with various aggregates. *J. Cem. Concr. Res.* **2012**.
50. Wang, Y.; Huang, J.; Wang, D.; Liu, Y.; Zhao, Z.; Liu, J. Experimental study on hygrothermal characteristics of coral sand aggregate concrete and aerated concrete under different humidity and temperature conditions. *Constr. Build. Mater.* **2020**, *230*, 117034. [CrossRef]
51. Payam, S.; Iman, A.; Norhayati, B. Concrete as a thermal mass material for building applications—A review. *J. Build. Eng.* **2018**, *19*, 14–25.
52. Lee, Y.H.; Chua, N.; Amran, M.; Yong Lee, Y.; Hong Kueh, A.B.; Fediuk, R.; Vatin, N.; Vasilev, Y. Thermal performance of structural lightweight concrete composites for potential energy saving. *J. Cryst.* **2021**, *11*, 461. [CrossRef]

53. Cao, V.D.; Pilehvar, S.; Salas-Bringas, C.; Szczotok, A.M.; Bui, T.Q.; Carmona, M.; Rodriguez, J.F.; Kjøniksen, A.-L. Thermal performance and numerical simulation of geopolymer concrete containing different types of thermoregulating materials for passive building applications. *Energy Build.* **2018**, *173*, 678–688. [CrossRef]
54. Saboor, S.; Chelliah, A.; Gorantla, K.; Kim, K.-H.; Lee, S.-H.; Shon, Z.H.; Brown, R.J.C. Strategic design of wall envelopes for the enhancement of building thermal performance at reduced air-conditioning costs. *J. Environ. Res.* **2021**, *193*, 110577. [CrossRef]
55. Asadi, I.; Shafigh, P.; Hassan, Z.F.B.A.; Mahyuddin, N.B. Thermal conductivity of concrete—A review. *J. Build. Eng.* **2018**, *20*, 81–93. [CrossRef]
56. Choktaweekarn, P.; Saengsoy, W.; Tangtermsirikul, S. A model for predicting the specific heat capacity of fly-ash concrete. *J. Sci. Asia* **2009**, *35*, 178–182. [CrossRef]
57. Robati, M.; McCarthy, T.J.; Kokogiannakis, G. Incorporating environmental evaluation and thermal properties of concrete mix designs. *J. Constr. Build. Mater.* **2016**, *128*, 422–435. [CrossRef]
58. Ruijun, W.; Ningning, Y.; Yang, L. Methods for improving the microstructure of recycled concrete aggregate: A review. *Constr. Build. Mater.* **2020**, *242*, 118164.
59. Zhengrong, L.; Dongkai, Z.; Cui, L. Experimental evaluation of indoor thermal environment with modularity radiant heating in low energy buildings. *Int. J. Refrig.* **2021**, *123*, 159–168.